Proceedings of the 21st ICSMGE, Vienna, Austria, 14 – 19 June 2026. Pistrol, Adam & Schweiger (eds.)
Published by: ÖGG, Austrian Society for Geomechanics, Salzburg, Austria, ISBN 978-3-9503898-4-5
https://doi.org/10.53243/ICSMGE2026-2326

X-ray CT Imaging of Internal Erosion in Sand with Loose Zones Under Seepage Flow

Shintaro Nohara
Central Research Institute of Electric Power Industry, Chiba, Japan, nohara-s@criepi.denken.or.jp

Toshifumi Mukunoki
Faculty of Advanced Science and Technology, Kumamoto University, Kumamoto, Japan

ABSTRACT: A laboratory experiment was conducted to clarify the internal erosion mechanism in sand with weak zones, such as cracks, under infiltration conditions. Referring to the hole erosion test (HET), the experiment involved preparing homogeneous specimens made of mixed sand and clay, as well as specimens with a loose zone, named coarse soil pipe (CSP), preset in the center of the mixed sand. The water flow rate was incrementally increased to measure the changes in the hydraulic gradient and conductivity during the flow, and the turbidity of the recovered water was also measured. Additionally, after the water flow, the sand specimens were visualized using microfocus X-ray computed tomography (CT), and image processing was performed to investigate the changes in the internal state due to the water flow. Laboratory experiments showed that clay flowed out of all the specimens when water passed through them. The hydraulic conductivity increased as the water flow rate increased. However, in specimens with a CSP, high turbidity of the water passing through the sand was observed, which indicates a large amount of clay flowing out. In addition, image processing of the CT images was performed to calculate the changes in gray values from the CT images taken in the previous stage, and differences were observed in the internal structures of the two specimens. In the homogeneous specimen, the gray values changed overall, but the particle flow path was unclear, suggesting limited migration of fine particles. By contrast, in the CSP specimen, the gray values changed significantly in the CSP and surrounding areas, confirming the internal erosion caused by the CSP pathway. However, as the flow rate increased, changes in the gray values were observed in areas other than the CSP.

KEYWORDS: X-ray CT, Hole erosion test, Seepage flow, Image processing.

1 INTRODUCTION

River embankments and fill dams are soil structures made of unconsolidated soil materials. Internal erosion caused by seepage can lead to the loss of soil particles, which can destabilize the structure. Weak areas, such as cracks inside the structure, are susceptible to internal erosion (Bridle, 2021). Erosion along the inner wall of the crack can result from the concentrated flow in weak areas, potentially leading to destruction. In the seismic performance assessment of fill dams in Japan, it is important to evaluate the internal erosion of weak areas when earthquakes may cause a slip surface to form at a depth greater than the dam water level (National Institute for Land and Infrastructure Management, 2005).

Previous studies have focused on the internal erosion in weak areas of sand structures by conducting a laboratory experiment called a hole erosion test (HET). In the HET, a hole several millimeters in diameter is placed in the center of a cylindrical soil specimen. Water is flowed in a direction parallel to the hole to evaluate the internal erosion. The pressure and flow rate during the water flow are measured. Then, the expansion of the central hole and turbidity of the drainage after the water flow are measured to evaluate the erosion resistance. As it is a simple experimental method, the HET has many applications. Research to derive theoretical solutions and numerical analyses of the HET experiment have been conducted (Bonelli et al. 2006; Benaissa et al. 2012; Cai et al. 2023). Furthermore, HET experiments were conducted using samples collected from embankments to evaluate their resistance to internal erosion (Jalil et al. 2012). However, further research is required because many unknowns remain regarding the internal erosion in weak areas and their surroundings.

In this study, a constant-flow seepage experiment was conducted on sand specimens with loose zones based on the HET experiment. The internal state of the specimens after water injection was visualized using microfocus X-ray computed tomography (CT), and image processing was conducted on the CT images to investigate the fine-particle outflow process and erosion mechanism in the specimens of sand containing weak areas.

2 CONSTANT FLOW SEEPAGE EXPERIMENT

The experimental apparatus used in this study is shown in Figure 1. The cylindrical acrylic column used in this experiment had an inner diameter of 50 mm and a height of 160 mm. A mixture of silica sand (D_{50} = 450 μm) and clay (DL clay) with a weight ratio of 8.5:1.5 was divided into five layers with a void ratio of 0.36 and packed into the acrylic column. The specimens were prepared without adjusting the moisture content, and the natural moisture content of sand was used.

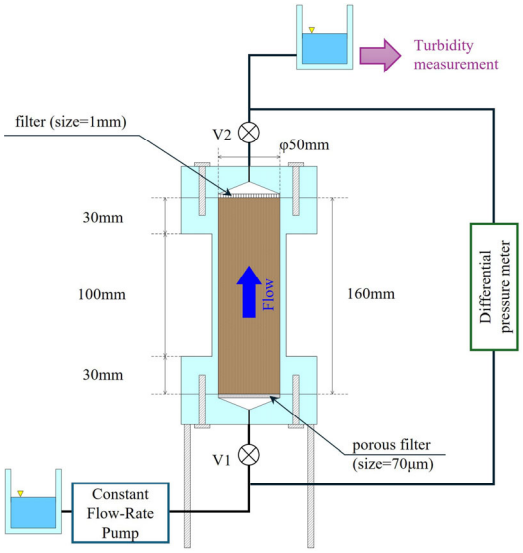

Figure 1. Experimental equipment.

The experiments were conducted using two types of specimens. Case A was a specimen created by filling the column with mixed sand to make it homogeneous, whereas Case B was a specimen that had a loose zone, hereinafter

referred to as coarse soil pipe (CSP), in the center of the mixed sand. To create the Case B specimen, a pipe with a diameter of 5 mm was installed near the center of the column. Then, the mixed sand was filled around the pipe. Next, the pipe was filled with silica sand and lightly compacted. Finally, the pipe was removed to simulate a loose zone. However, because it was difficult to continuously prepare specimens with the CSP up to the top of the column, an area approximately 5 mm below the top of the column was filled with mixed sand only.

The first step after filling the column with sand was to saturate the column. This was achieved by flowing degassed distilled water at a rate of 0.10 mL/min using a constant-flow pump in the vertical upward direction. The flow rate was set to approximately four times the pore volume during this stage (approximately 400 mL). During water flow, a differential pressure gauge was used to measure the pressure difference between the upstream and downstream sections of the column. The initial saturated hydraulic conductivity was calculated based on the differential pressure measurement results for approximately 1 h before the water flow was stopped.

Subsequently, the flow rate was gradually increased to 0.20, 0.50, and 0.80 mL/min. Degassed distilled water was then passed through the column at each flow rate until the volume passed through was approximately twice the pore volume (approximately 200 mL). All the water that drained from the column was collected, and its turbidity was measured using a turbidity meter after the water flow stopped. After a specified amount of water was passed through, the pump was turned off, the tube was removed, and the column base was attached to the turntable of a CT device to prevent the specimen from shifting positions, as shown in Figure 2. CT was then performed. The CT scanning was conducted with a tube voltage of 130 kV and a tube current of 250 μA. The CT images acquired in the three vertical directions were combined.

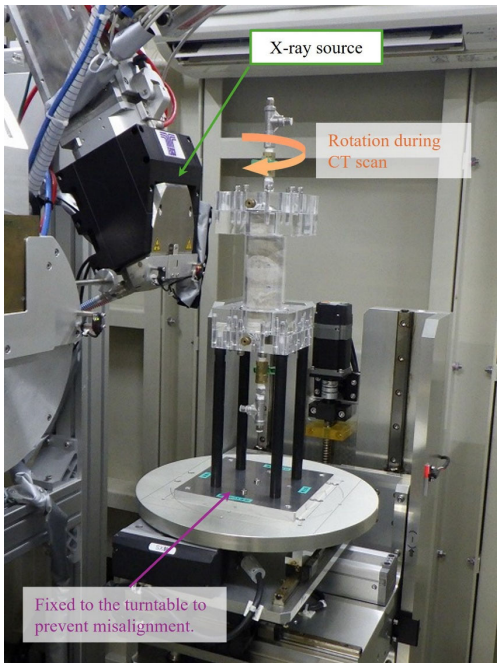

Figure 2. Computed tomography (CT) scanning of the sand column.

3 EXPERIMENTAL RESULTS

The results of measuring the turbidity of the water passing through the sand column are shown in Figure 3. There was no difference in the turbidity of the water used to increase saturation in either Case A or Case B. However, differences appeared in both cases as the flow rate increased. The turbidity of Case B, with the CSP placed at the center, was consistently higher than that of Case A, which used a homogeneous specimen. The turbidity peaked at 0.20 mL/min and then gradually decreased. When the passed water was visually inspected, no large sand particles such as silica sand were observed. Therefore, the increase in the turbidity of the drained water was due to the flow of clay particles out of the column.

Figure 4 shows the results of calculating changes in the hydraulic gradient and hydraulic conductivity over time based on differential pressure gauge measurements. In both cases, the horizontal axis represents the volume of water flowing through the specimen from the start of the injection at each set flow rate, which was calculated from the flow rate and elapsed time.

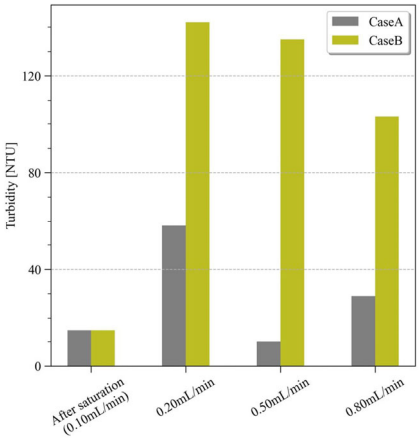

Figure 3. Turbidity measurement results.

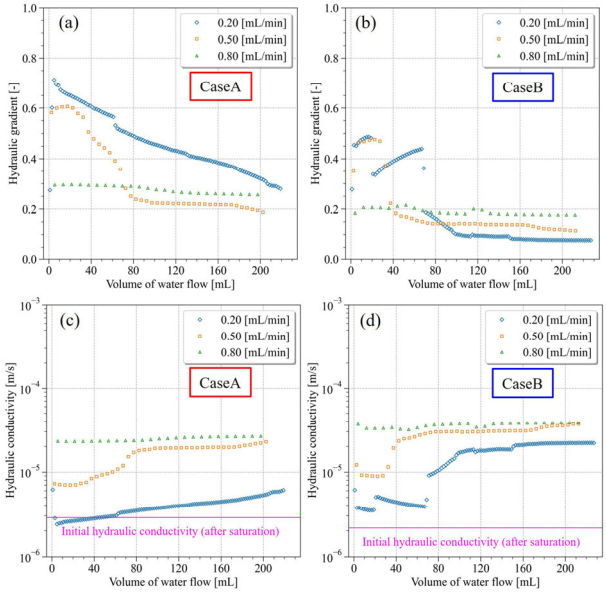

Figure 4. Changes in hydraulic gradient and hydraulic conductivity.

The hydraulic conductivity of Case B, which had a loose zone at the center, was predicted to be higher than that of Case A, which was a homogeneous specimen. However, in this experiment, the initial hydraulic conductivity was 2.84×10^{-6} m/s for Case A and 2.33×10^{-6} m/s for Case B, with no significant difference observed between them. This is owing to the non-continuity of the CSP in the direction parallel to the flow. In future studies, it will be necessary to improve the method of preparing specimens such that the CSP is continuous.

In general, when no internal erosion and no significant structural changes were observed, the hydraulic gradient increased linearly with the injection flow rate, and the hydraulic conductivity remained constant. In this experiment, however, both the hydraulic gradient and hydraulic conductivity changed

significantly during water flow. This change is thought to be related to clay outflow. The final hydraulic conductivity was 2.65×10^{-5} m/s for Case A and 3.84×10^{-6} m/s for Case B. Both values were approximately one order of magnitude higher than the initial values.

4 CT IMAGES

The CT image of Case B with the CSP in the center, captured after the specimen was prepared (before saturation), is shown in Figure 5. The image size is 1,800 × 1,800 × 3,798 voxels, and the voxel size is 30 µm/voxel. Figure 5 (a) and (b) show YZ and XY cross-sectional views of the entire specimen, respectively. Figure 5 (c) and (d) are enlarged views of the CSP in the center. Figure 5 (a) shows dark areas at the top and bottom, which are artifacts caused by the flange of the acrylic column. The CT images show clay particles filling the gaps between the silica sand. Additionally, a CSP section consisting of a 5 mm outer diameter pipe filled with silica sand was identified.

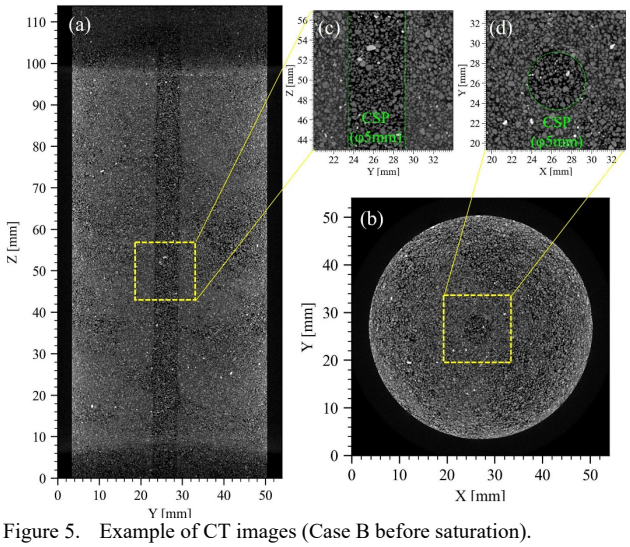

Figure 5. Example of CT images (Case B before saturation).

5 IMAGE PROCESSING

Image processing of the CT images was performed to clarify the changes in the internal structure of sand induced by water flow. First, a grid of 40 voxels (1.2 mm) per side was generated on the CT image. Then, the average gray value of the voxels within the grid was calculated. The grid size was determined by considering the positional shift caused by column repositioning and the voxel size. Next, the difference between the average gray values of each grid and those of the previous stage was calculated. Figure 6 and Figure 8 show enlarged CT images of Case A and Case B, respectively. Figure 7 and Figure 9 show the results obtained by subtracting the average gray values calculated at each grid before the flow rate changes from the average gray values calculated after the flow rate changes in Case A and Case B, respectively. Because the gray values in CT images generally correlate with density, an increase in gray values indicates reduced porosity owing to the inflow of sand or clay caused by water flow. In contrast, a decrease in gray values indicates increased porosity owing to the outflow of sand or clay caused by the water flow.

No significant changes in the internal structure owing to internal erosion were observed on the enlarged CT image. Furthermore, even in Case B, where the CSP was placed in the center, no significant erosion of the CSP wall surface was observed, and the shape of the hole appeared to have been maintained. However, when calculating the change in the gray value, it became clear that different changes occurred in Cases A and B. As shown in Figure 7, in Case A (the homogeneous specimen), a complex mixture of areas where the gray value increased and decreased was observed, and no clear outflow path was observed. This suggests that even if sand and clay are transported by water flow, they become trapped in downstream voids, and the movement of particles is limited to a short distance.

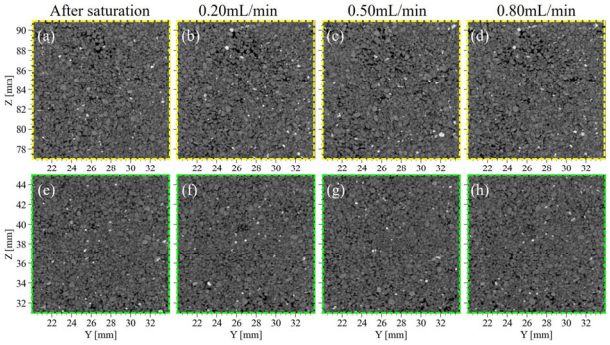

Figure 6. Enlarged CT image of Case A.

The upper section indicates the upper part of the column (downstream), and the lower section indicates the lower part of the column (upstream).

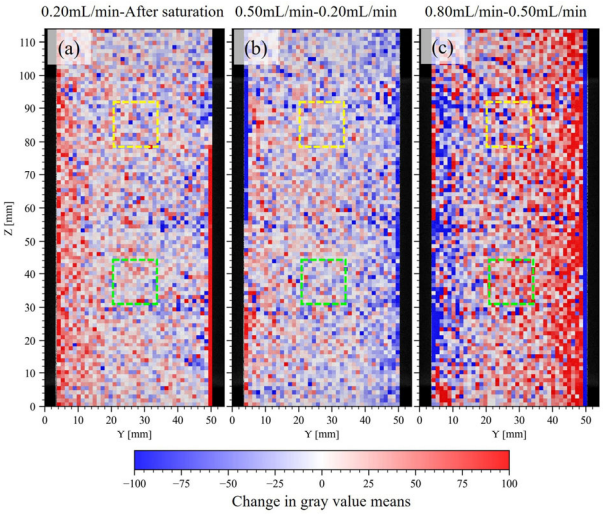

Figure 7. Difference calculation results for two images of Case A.

The calculation result was obtained by subtracting the average gray value image taken after the flow rate change from the average gray value image taken before the flow rate change. The dotted lines (yellow and green) correspond to the enlarged images shown in Figure 6.

In Case B, which had a CSP in the center, different changes were observed at each step. When the flow rate was 0.20 mL/min, a region of reduced gray values was observed along the flow direction in the CSP zone (Figure 9 a). These changes were related to the particles flowing into the CSP zone in the previous stage and being discharged outside the column, as well as the erosion progression on the CSP wall. In addition, changes in gray values were observed in zones other than the CSP zone. At a flow rate of 0.50 mL/min, an area of increased gray value along the flow direction was observed in the CSP region (Figure 9 b). Meanwhile, the gray value remained almost unchanged in the regions outside the CSP. The gray value decreased in the lower (upstream) part of the column, suggesting that the sand and clay in this region were transported to the upper (downstream) part by the upward flow. Although

significant changes in the gray values were mainly observed in the CSP until this stage, when the water flow rate reached 0.80 mL/min, changes were observed not only in the CSP but also in the overall specimen, transitioning to changes similar to those in Case A (Figure 9 c). Figure 10 shows that such changes occurred not only in the YZ section, but also throughout the entire specimen. This indicates that the CSP corresponds to the sand and clay flow path.

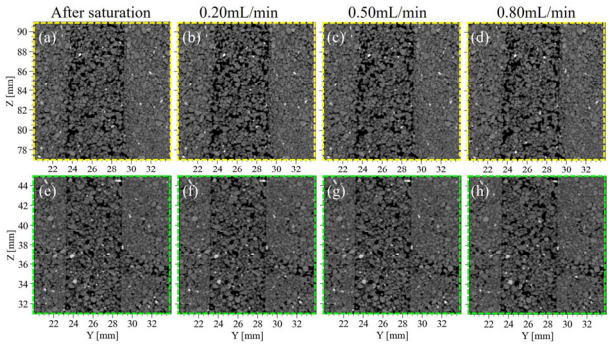

Figure 8. Enlarged CT image of Case B.

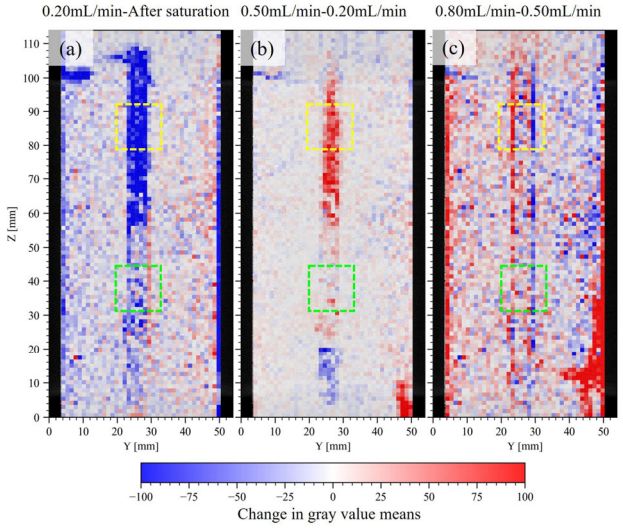

Figure 9. Difference calculation results for two images of Case B.

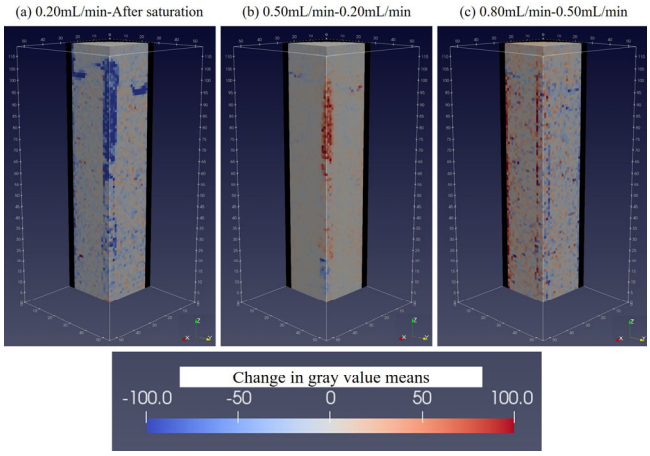

Figure 10. Image processing results in Case B (3D).

As confirmed by the above experiments, when weak zones exist in soil structures, sand and clay particles move in and around the weak zones, causing internal erosion. However, it was found that internal erosion occurred not only in the weak zones. Complex processes are involved, and depending on the flow velocity, internal erosion may occur in areas other than weak zones owing to the movement of sand and clay particles.

6 CONCLUSIONS

This paper presents HET experiments performed in the laboratory to evaluate the internal erosion of soils with weak zones. The laboratory experiments involved obtaining CT images of sand specimens after water flow using microfocus X-ray CT. Image processing was performed to study the fine particle outflow and internal erosion mechanisms.

As a result, the differences in the internal changes between the homogeneous specimens and specimens containing weak zones were confirmed. Additionally, it was confirmed that when weak zones exist, internal erosion around these zones is the primary factor. However, depending on the flow velocity, the fine particles can be washed away from other areas, thereby causing internal erosion. Future studies should focus on improving the specimen preparation method and increasing the number of experimental conditions to thoroughly investigate the detailed internal erosion process in weak zones.

7 REFERENCES

Benaissa, K., Angel, P.V.M., Dlolores, R.C.M., Philippe, D., Abdellatif, K., Mohammed, B., and Larbi, E.B. 2012. Predicting initial erosion during the hole erosion test by using turbulent flow CFD simulation, *Applied Mathematical Modelling*, 36, 8, 3359-3370.

Bonelli, S., Benahmed, N., and Brivois, O. 2006. On Modelling of the Hole Erosion Test, *3rd International Conference on Scour and Erosion*, Amsterdam.

Bridle, R. 2021. Applying Internal Erosion Mechanics to improve Internal Erosion Risk Assessments, *10th International Conference on Scour and Erosion*.

Cai, W., Bora, M.J., Pekkat, S., Bordoloi, S., Garg, A., and Sekharan, S. 2023. A new and simple model for predicting soil erosion based on hole erosion tests, *Acta Geophysica*, 7, 2, 823-836.

Jalil, A., Benamar, A., and Touhami, M. 2012. Predicting initial erosion during the hole erosion test by using turbulent flow CFD simulation, *Applied Mathematical Modelling*, 36, 8, 3359-3370.

National Institute for Land and Infrastructure Management (NILIM). 2005. Technical note on seismic performance evaluation of dams against large earthquake (in Japanese).